Available online at www.sciencedirect.com
SCIENCE DIRECT
Biochemical and Biophysical Research Communications 345 (2006) 210–215
BBRC
www.elsevier.com/locate/ybbrc

Selective destabilization of soluble amyloid β oligomers by divalent metal ions

K. Garai, P. Sengupta [1], B. Sahoo, S. Maiti *

Tata Institute of Fundamental Research, Homi Bhabha Road, Colaba, Mumbai 400005, India

Received 11 April 2006
Available online 25 April 2006

Abstract

Aggregation of the amyloid β (Aβ) peptide yields both fibrillar precipitates and soluble oligomers, and is associated with Alzheimer's disease (AD). In vitro, Cu^{2+} and Zn^{2+} strongly bind Aβ and promote its precipitation. However, less is known about their interactions with the soluble oligomers, which are thought to be the major toxic species responsible for AD. Using fluorescence correlation spectroscopy to resolve the various soluble species of Aβ, we show that low concentrations of Cu^{2+} (1 μM) and Zn^{2+} (4 μM) selectively eliminate the oligomeric population (within ~2 h), while Mg^{2+} displays a similar effect at a higher concentration (60 μM). This uncovers a new aspect of Aβ–metal ion interactions, as precipitation is not substantially altered at these low metal ion concentrations. Our results suggest that physiological concentrations of Cu^{2+} and Zn^{2+} can critically alter the stability of the toxic Aβ oligomers and can potentially control the course of neurodegeneration.

Keywords: Amyloid β; Oligomers; Oligomer–metal ion interaction; Protein aggregation; Alzheimer's disease

Deposition of the amyloid β peptide in the brain is a pathological hallmark of Alzheimer's disease (AD) [1]. In vitro, Zn^{2+} and Cu^{2+} bind $A\beta_{1-40}$ with binding constants of ~5 μM and ~15 nM, respectively [2–4]. These divalent cations also increase the rate of Aβ aggregation by 100- to 1000-fold when present at more than 100 μM concentration [5]. In vivo, these metal ions co-precipitate with Aβ and have been suspected to play a role in AD pathology [6,7].

However, the soluble oligomeric species of Aβ are now believed to be the dominant agents of Aβ neurotoxicity [8–14]. The soluble Aβ load in the brain, especially that of $A\beta_{1-40}$, has been found to be a better predictor of the severity of AD compared to the amount of insoluble Aβ deposits [15]. If metal ions do play a role in AD, it is likely that they affect these oligomeric species, but very little is known about such interactions. Here, we investigate how the different soluble species of Aβ are perturbed by different divalent cations, viz., Zn^{2+}, Cu^{2+}, and Mg^{2+}, at various concentrations. We also probe the kinetics of these perturbations.

Various scattering (dynamic light scattering, small angle neutron scattering) [16,17], size exclusion chromatography [18], and imaging techniques (atomic force microscopy and electron microscopy) [9,16,19] have been used to characterize the Aβ oligomers in vitro. Depending on the method of preparation and characterization, several soluble species of Aβ have been detected. They have been classified into low molecular weight (LMW) oligomers (up to 6-mer, 2–3 nm), spherical oligomers (8–10 nm or larger), and protofibrils or large oligomers (~50 nm) [9,10,16,18]. We have shown that fluorescence correlation spectroscopy (FCS) [20,21], together with the MEMFCS data analysis algorithm [22], is a sensitive optical technique for resolving aggregate sizes in a solution. FCS makes it possible to measure the size distribution in the solution state over a wide range of sizes (from monomers to the largest soluble particles) and concentrations (from nM to mM), with a good time resolution (~1 min). Aβ oligomers of different sizes, corresponding to some of the species found with other techniques, have been

* Corresponding author. Fax: +91 22 2280 4610.
E-mail address: maiti@tifr.res.in (S. Maiti).
[1] Present address: Physiology and Biophysics, Basic Health Sciences, T6-192, State University of New York, Stony Brook, NY 11794-8661, USA.

0006-291X/$ - see front matter © 2006 Elsevier Inc. All rights reserved.
doi:10.1016/j.bbrc.2006.04.056

observed by FCS [23]. Here, we employ FCS to study the effects of Cu^{2+}, Zn^{2+}, and Mg^{2+} at several concentrations on each of the soluble species of Aβ.

Theory

Fluorescence correlation spectroscopy

The measured variable for FCS experiments is the temporal autocorrelation $G(\tau)$ of the fluorescence fluctuation, which is defined as

$$G(\tau) = \frac{\langle \delta F(t) \delta F(t+\tau) \rangle}{\langle F(t) \rangle^2}, \quad (1)$$

where $\delta F(t)$ is the fluctuation in fluorescence at time t about the average fluorescence $\langle F(t) \rangle$ [21]. $G(\tau)$ is related to the characteristic time τ_D for a particle to diffuse through the probe volume. For a three-dimensional Gaussian-shaped probe volume (a reasonable approximation to our experimental setup) with r and l as the characteristic radial and axial dimensions (i.e., where the Gaussian function drops to $1/e^2$ of its value at the maximum), $G(\tau)$ for a solution with n non-interacting fluorescent species is given by [22]

$$G(\tau) = \sum_{i=1}^{n} b_i \left(\frac{1}{1 + (\tau/\tau_{D_i})} \right) \left[\frac{1}{1 + (r/l)^2 (\tau/\tau_{D_i})} \right]^{1/2}, \quad (2)$$

where $\tau_{D_i} = r^2/4\, D_i$, D_i is the diffusion constant (inversely proportional to the hydrodynamic radius of the species i) and b_i is the relative weight of ith component. b_i is directly proportional to the concentration and also to the square of the brightness of the species i [21].

Obtaining the size distribution from FCS data

Conventional models used to fit FCS data assume a small number of diffusing species and are adequate for describing simple systems with limited heterogeneity. Such an approach is inadequate for extracting physically meaningful inferences from an aggregating protein solution where a large number of species of different sizes may coexist. We use a maximum entropy method-based data analysis algorithm (MEMFCS) [22]. This, using Eq. (2), interprets the data in terms of a quasi-continuous distribution of particle sizes (here we use 150 components) and yields the widest possible size distribution that is consistent with the data. To follow the kinetics of aggregation, we make repeated FCS measurements in time (starting from the time of preparing the solution) and assume that the kinetics are slow enough so that the system can be considered to be in a quasi-equilibrium state during each FCS measurement.

Materials and methods

Preparation of Aβ solutions for FCS measurements. $A\beta_{1-40}$ was purchased from American Peptide Company (Sunnyvale, CA) and rhodamine-labeled $A\beta_{1-40}$ ($RA\beta_{1-40}$) was purchased from RPeptide (Athens, GA). Powdered Aβ was weighed and directly dissolved in Hepes buffer [compositions 20 mM Hepes (Sigma–Aldrich, MO), 150 mM NaCl, and 5 mM KCl] at pH 7.4. All salts used were recrystallized twice in distilled water to eliminate trace impurities. To probe the effect of the metal ions on Aβ aggregation, a Hepes-buffered solution containing 60 μM $A\beta_{1-40}$ and 100 nM $RA\beta_{1-40}$ (the latter is a reporter molecule present at low concentrations) is prepared and distributed in different aliquots. At this concentration the solutions are initially supersaturated, and visible precipitates are observed within 2 days. Freshly prepared aliquots are incubated with different concentrations of Zn^{2+}, Cu^{2+} or Mg^{2+} (all added as their respective chloride salts) for 48 h. The concentrations of the metal ions used do not exceed their solubility in Hepes as was confirmed by scattering measurements performed on the solutions using a fluorimeter (Fluoromax-3, Jobin Yvon Horiba, Edison, NJ). All the solutions are then centrifuged at 2000*g* for 20 min to get rid of heterogeneous large particles present in the solutions, and the supernatants are taken for FCS studies.

FCS measurements. FCS experiments are performed with a home-built spectrometer using single-photon excitation as described elsewhere [24]. Briefly, the experimental setup consists of a high-numerical aperture objective lens (60×, 1.2 NA, water immersion, Nikon, Melville, NY), which focuses a continuous wave green He–Ne laser (1.2 mW at 543.5 nm, Jain Laser Technology, Mumbai, India) beam into the sample. The laser power at the objective back aperture is kept typically below 100 μW. Fluorescence is collected through the same microscope objective, separated from the excitation light by both a dichroic mirror (560DCLP, Chroma Inc., Brattleboro, VT) and an emission filter (585DF40, Chroma Inc., VT), and focused with an achromat lens ($F = 150$ mm, Newport, Irvine, CA) onto a multimode fiber (50 μm core diameter, Newport). The other end of the fiber is connected to a fiber-coupled APD detector (SPCM-AQR-150, Perkin-Elmer, Fremont, CA). The detector signal is then processed with an autocorrelator card (ALV5000E, ALV Laser VmbH, Langen, Germany). The correlation decay traces are then fitted with Eq. (2) using the MEMFCS algorithm [22].

Measurement of Aβ content in the solution. $A\beta_{1-40}$ has a tyrosine residue at the 10th position whose fluorescence is used as a measure of the Aβ concentration in the solution. The tyrosine residue is excited at 285 nm and the emission spectra are recorded from 295 to 350 nm.

Results

Size distribution in an aggregating Aβ solution

We use fluorescence correlation spectroscopy (FCS) to measure the total size distribution of the soluble particles present in a 60 μM Aβ solution, soon after the preparation of the solution. The FCS data with the fit (obtained using the MEMFCS fitting routine [22]) are shown in Fig. 1A (stars), where the abscissa corresponds to the delay time and the ordinate corresponds to the normalized autocorrelation value (see Eq. (1)). The size distribution obtained from the fit is shown in Fig. 1B (stars). Here, the abscissa indicates the hydrodynamic size of the particles in nanometers, and the ordinate represents the population weighted by the square of the particle brightness (see Eq. (2)). The size axis is calibrated using Rhodamine B (hydrodynamic radius = 0.78 nm) as a standard (filled squares, Fig. 1B). The size distribution shows three predominant peaks. The first peak contains particles from 1.2 to 3.0 nm. The estimated size of an Aβ monomer is 1.6 nm, hence this peak primarily contains monomers and low molecular weight oligomers. The second peak ranges from 50 to 120 nm

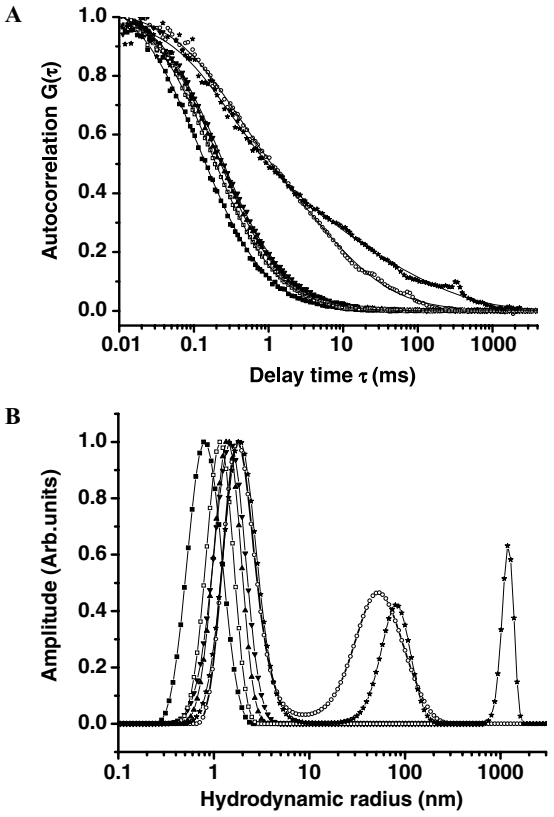

Fig. 1. Effect of Zn^{2+} on the particle size distribution of an Aβ solution. (A) Fluorescence autocorrelation data (discrete symbols) as a function of delay time with the corresponding fitted curves (continuous lines). Freshly prepared Aβ without centrifugation (stars); Aβ centrifuged 48 h after preparation (open circles); Aβ incubated with 4 μM Zn^{2+}, centrifuged 48 h after preparation (upright triangles); similar preparation incubated with 50 μM Zn^{2+} (inverted triangles); and 600 μM Zn^{2+} (open squares); Rhodamine B in buffer (filled squares). (B) The particle size distribution obtained from fitting of the data in (A). The abscissa is calibrated using Rhodamine B as a standard. The ordinate represents concentration weighted by the square of the particle brightness.

particles which are the larger oligomers. The third peak shows even bigger particles (>1 μm). The particles in this size range are too large to be sustained in the solution, and they precipitate in the time scale of minutes to hours.

Effect of metal ions on a quasi-stable Aβ solution

We then investigate the effect of Zn^{2+}, Cu^{2+}, and Mg^{2+} ions on the different soluble species of Aβ. A solution containing 60 μM Aβ is incubated for 48 h at room temperature with these metal ions at various concentrations. Finally, the solutions are centrifuged for 20 min at 2000*g* to precipitate any insoluble species and the supernatants are collected for FCS measurements.

We use Zn^{2+} concentrations of 4, 50, and 600 μM, and also record data from a rhodamine solution and a control Aβ solution (without any metal ions added). Fig. 1A shows the FCS data with the fit and Fig. 1B shows the size distribution obtained from these solutions. The control solution shows two peaks (Fig. 1B, open circles). The first peak extends from 1.0 to 3.5 nm, clearly indicating the presence of the monomers and the LMWs and the second peak extends from 20 to 130 nm, indicating protofibrils or larger oligomers or both. Remarkably, even with the lowest concentration of Zn^{2+} (4 μM), the larger species disappear and only the monomer-like species remain (Fig. 1B, upright triangles).

Similar experiments are performed with Cu^{2+} in the buffer at concentrations of 1, 10, and 100 μM. The FCS data with the fit and the size distribution are presented in Fig. 2A and B, respectively. The dataset shows the control specimen (open circles), and specimens containing 1 μM Cu^{2+} (upright triangles), 10 μM Cu^{2+} (inverted triangles), and 100 μM Cu^{2+} (open squares), respectively. It can be seen that Cu^{2+} also makes the larger oligomers disappear even at the lowest concentration used (1 μM).

The results obtained from solutions containing Mg^{2+} at concentrations of 0 μM (open circles), 4 μM (upright triangles), 60 μM (inverted triangles), and 1 mM (open squares) are shown in Figs. 3A and B. Fig. 3A presents the FCS data with the corresponding fit and Fig. 3B presents the particle size distributions. The size distribution obtained

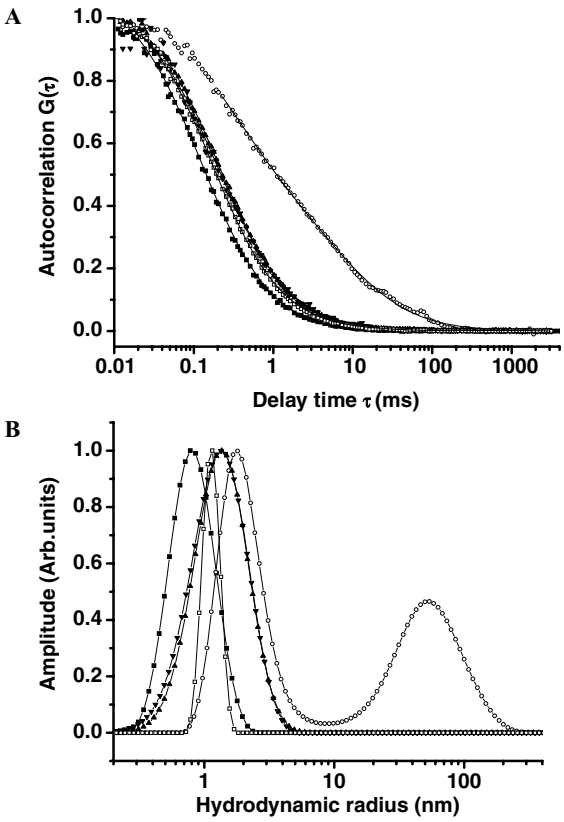

Fig. 2. Effect of Cu^{2+} on the particle size distribution of an Aβ solution. (A) Fluorescence autocorrelation data (discrete symbols) as a function of delay time with the corresponding fitted curves (continuous lines). Aβ centrifuged 48 h after preparation (open circles); Aβ incubated with 1 μM Cu^{2+}, centrifuged 48 h after preparation (upright triangles); similar preparation incubated with 10 μM Cu^{2+} (inverted triangles); and 80 μM Cu^{2+} (open squares); Rhodamine B in buffer (filled squares). (B) The particle size distribution obtained from fitting of the data in (A).

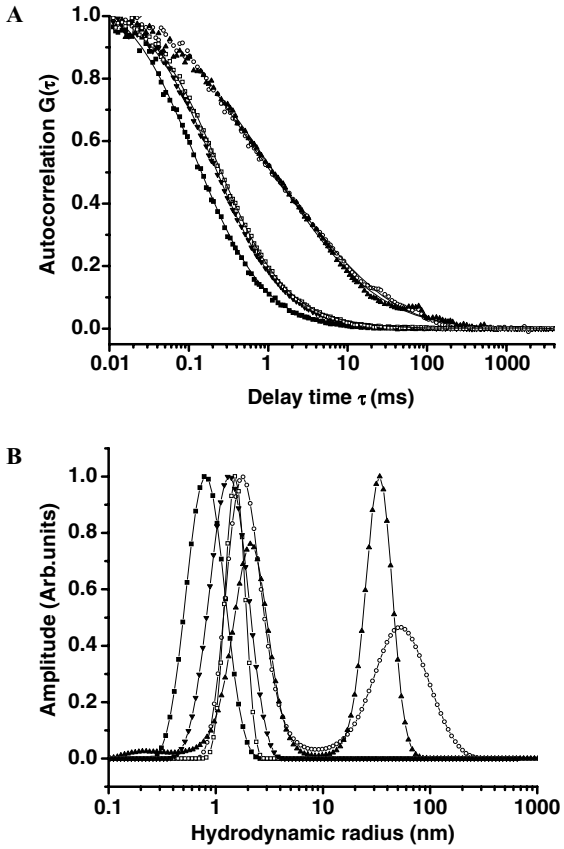

Fig. 3. Effect of Mg^{2+} on the particle size distribution of an Aβ solution. (A) Fluorescence autocorrelation data (discrete symbols) as a function of delay time with the corresponding fitted curves (continuous lines). Aβ centrifuged 48 h after preparation (open circles); Aβ incubated with 4 μM Mg^{2+}, centrifuged 48 h after preparation (upright triangles); similar preparation incubated with 60 μM Mg^{2+} (inverted triangles); and 1 mM Mg^{2+} (open squares); Rhodamine B (filled squares). (B) The particle size distribution obtained from fitting of the data in Fig. 1A.

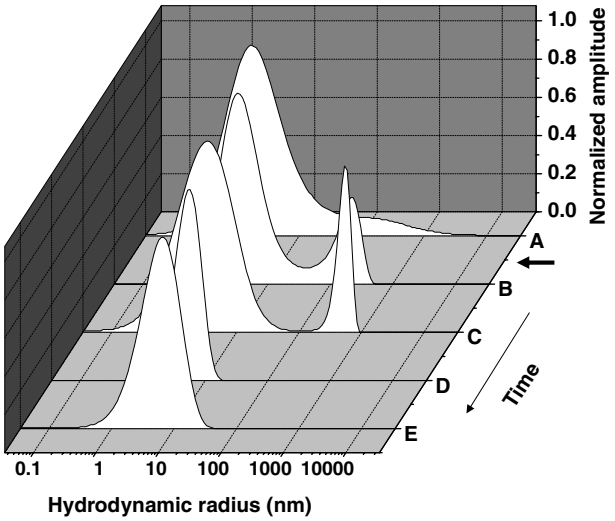

Fig. 4. Evolution of the size distribution of an Aβ solution after addition of 1 μM of Cu^{2+}. (A) Before addition of Cu^{2+}, it shows monomer and oligomers (the tail of the distribution). The black thick arrow shows the time at which 1 μM Cu^{2+} is added. (B) After 45 min of Cu^{2+} addition; (C) after 1 h of Cu^{2+} addition; (D) after 2 h of Cu^{2+} addition and (E) after two and a half an hour of Cu^{2+} addition.

from the Aβ solution incubated with 4 μM Mg^{2+} (upright triangles) shows both the peaks unlike the solutions incubated in presence of similar concentrations of Zn^{2+} and Cu^{2+}. 60 μM and 1 mM of magnesium make the oligomers disappear (inverted triangles and open squares, respectively). The solutions in which the oligomers disappear also show a narrowing and leftwards shift of the first peak, which indicates a simultaneous decrease of the LMW populations in these solutions. The second peak actually appears to grow upon incubation with 4 μM Mg^{2+}. However, while the position of a peak in MEMFCS analysis is robust, its height and width can vary somewhat depending on the errors of the data [22]. Therefore, the growth of the second peak may not be significant.

Kinetics of disappearance of the oligomers

The results shown above are obtained from Aβ solutions incubated with metal ions for ~2 days. We investigate whether the actual disappearance of the oligomers occurs at a faster time scale. We add 1 μM Cu^{2+} to an Aβ solution containing the oligomers and record FCS data every 3 min. Fig. 4 shows the time development of the particle size distribution from the Aβ solution before and after the addition of Cu^{2+}. Initially, in the absence of the metal ions, the particle distribution is broad and its tail extends up to ~1 μm. Within 45 min of application of Cu^{2+}, the initial broad distribution is separated into two parts. The first part, with a peak at 3 nm, is narrower than before and extends up to ~10 nm, while the second part represents larger particles and ranges from 100 to 400 nm. Within 2 h after the addition of the Cu^{2+}, the oligomeric peak completely disappears, and now the size distribution extends only up to ~10 nm. The oligomers do not reappear later (see time point *E*, 2.5 h).

Effect of metal ions on the solubility of Aβ

We further looked at the effect of these metal ions on the saturation concentration (i.e., the total solubility without regard to the soluble species) of Aβ by steady-state fluorimetry. The fluorescence at 305 nm upon excitation at 285 nm reports the fluorescence of the tyrosine residue at position 10 of Aβ and measures the total soluble Aβ present in the solutions. We can see from Fig. 5 that the total soluble Aβ content is not significantly affected by the presence of 1 μM Cu^{2+} or 4 μM Zn^{2+}. However, a similar experiment with 15 μM Aβ in the presence of 600 μM Zn^{2+} reveals that the soluble Aβ content after 2 days reduces by a factor of 10. Our results agree with the previous reports that Zn^{2+} and Cu^{2+} at low concentrations does not increase Aβ precipitation significantly, but reduces its solubility at higher concentrations (>100 μM) [5].

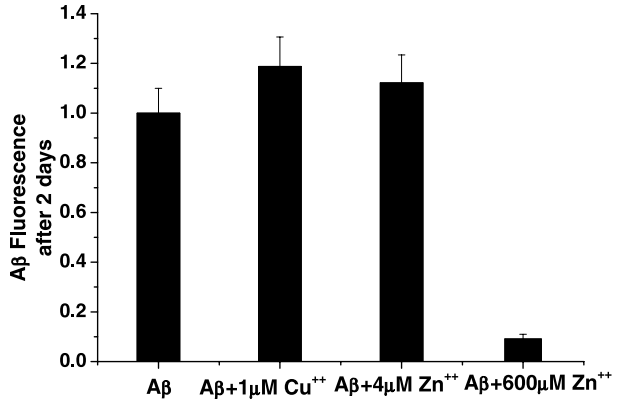

Fig. 5. Precipitation of Aβ by metal ions. The bar graph shows the total Aβ concentration remaining in solution, 2 days after preparation. Compared to plain buffer (normalized to unity), presence of 1 μM Cu^{2+} or 4 μM Zn^{2+} does not substantially alter Aβ precipitation, while 600 μM Zn^{2+} reduces it by a factor of ~10.

Discussions

To understand the effect of metal ions on AD, it is important to understand how metal ions interact with the monomers and various types of aggregates. To date, only the increased precipitation of Aβ by metal ions has been studied. It is not known whether there is any selectivity regarding the soluble species in this precipitation. The different types of soluble aggregates characterized in different experiments most likely have different levels of toxicity [8–14], so such selectively can be rather significant. It is likely that the supramolecular structure adopted by these different oligomers actually modulates their ability to bind metal ions. Therefore, in principle, metal ion binding can have very different effects on the stability of these individual species. FCS lets us uncover these effects systematically.

Copper and zinc make oligomers disappear

FCS measurements on the supernatant of a 60 μM Aβ solution after 48 h of preparation show the presence of oligomers in equilibrium with the monomers and LMWs (Fig. 2B, open circles). The hydrodynamic size of the oligomers lies within 20–130 nm. Oligomers of similar sizes have been reported earlier and have been characterized as protofibrils [16]. Application of 1 μM Cu^{2+} or 4 μM Zn^{2+} eliminate the oligomers (Fig. 2B and 1B, upright triangles). If there is substantial precipitation of all the soluble species of Aβ due to the presence of these metal ions, then such disappearance may not be remarkable. However, it can be seen from Fig. 5 that the saturation concentration of Aβ does not change within the experimental errors in presence of 1 μM Cu^{2+} or 4 μM Zn^{2+}. Our results thus show that the oligomers, a potent toxic species in AD, can be eliminated with the application of small concentrations of Zn^{2+} and Cu^{2+}, without substantially affecting the Aβ solubility. However, we do not know whether the oligomers disappear by dissociation or aggregation. The solubility measurements show no increase of overall precipitation in presence of Zn^{2+} and Cu^{2+}. This suggests that if the oligomers disappear by mutual aggregation, then their overall population must be too low to be detected by fluorimetry measurements. We note that a mechanistic explanation of why Cu^{2+} and Zn^{2+} are able to selectively precipitate the oligomeric species remains to be found.

Precipitation of the monomers and LMWs by metal ions at high concentrations

From Fig. 1B, 2B, and 3B it can be seen that the first peak containing the monomers and LMWs narrow down towards smaller sizes at the higher metal ion concentrations. The fluorimetry data in Fig. 5 suggest that the solubility of Aβ is considerably less at high Zn^{2+} concentrations. The overall precipitation is 90% more for 600 μM Zn^{2+} compared to solutions lacking Zn^{2+}. It is also known that 30 μM Cu^{2+} induces 20% more precipitation of Aβ [25]. Our observations thus suggest that the metal ions at high concentrations interact with all soluble Aβ species including the large and the small oligomers to form larger particles and promote precipitation. While Cu^{2+} and Zn^{2+} are known to specifically bind Aβ, the effect of Mg^{2+} is somewhat unexpected. It is possible that the Zn^{2+}- and Cu^{2+}-binding mechanism of Aβ (which is mediated by His (6), His (13), and His (14) [26–28]) also helps the binding of other divalent ions such as Mg^{2+} at high enough concentrations.

Possible physiological relevance

The normal concentrations of Zn^{2+} and Cu^{2+} in the cerebrospinal fluid are ~3 and ~1 μM, respectively [29], which are similar to the concentrations of the Cu^{2+} and Zn^{2+} we have used. During synaptic transmission, Zn^{2+} concentrations can reach 300 μM [30]. Zn^{2+} is found co-precipitated with Aβ in the amyloid plaques formed in the brain and is thus suspected to be potentially harmful in AD [6,7]. Instead, what we find suggests that Zn^{2+} (and Cu^{2+}) at such concentrations may actually be playing a beneficial role. The oligomers of ~50 nm range are known to be toxic [31]. Preferential precipitation of the oligomers may be the natural way of keeping the toxic oligomer population down in the brain. It is interesting to note that concentrations of Zn^{2+} and Cu^{2+} are found to be lower in the AD brains compared to the age-matched controls [29]. If the oligomeric species are primarily responsible for AD, then the ability of these ions to destabilize the oligomeric species can potentially be an important key for chemical intervention in AD.

Acknowledgments

S.M. is a Wellcome Trust Overseas Senior Research Fellow in Biomedical Sciences in India (Ref. No. 05995/Z/99/Z/HH/KO). K.G. and B.S. are recipients of Kanwal Rekhi

Career Development Scholarship of the Tata Institute of Fundamental Research.

References

[1] D.J. Selkoe, The molecular pathology of Alzheimer's disease, Neuron 6 (1991) 487–498.
[2] A.I. Bush, W.H. Pettingell Jr., M.D. Paradis, R.E. Tanzi, Modulation of A beta adhesiveness and secretase site cleavage by zinc, J. Biol. Chem. 269 (1994) 12152–12158.
[3] C.S. Atwood, R.C. Scarpa, X. Huang, R.D. Moir, W.D. Jones, D.P. Fairlie, R.E. Tanzi, A.I. Bush, Characterization of copper interactions with Alzheimer amyloid beta peptides: identification of an attomolar-affinity copper binding site on amyloid beta 1–42, J. Neurochem. 75 (2000) 1219–1233.
[4] A. Clements, D. Allsop, D.M. Walsh, C.H. Williams, Aggregation and metal-binding properties of mutant forms of the amyloid A beta peptide of Alzheimer's disease, J. Neurochem. 66 (1996) 740–747.
[5] P.W. Mantyh, J.R. Ghilardi, S. Rogers, E. DeMaster, C.J. Allen, E.R. Stimson, J.E. Maggio, Aluminum, iron, and zinc ions promote aggregation of physiological concentrations of beta-amyloid peptide, J. Neurochem. 61 (1993) 1171–1174.
[6] M.A. Lovell, J.D. Robertson, W.J. Teesdale, J.L. Campbell, W.R. Markesbery, Copper, iron and zinc in Alzheimer's disease senile plaques, J. Neurol. Sci. 158 (1998) 47–52.
[7] S.W. Suh, K.B. Jensen, M.S. Jensen, D.S. Silva, P.J. Kesslak, G. Danscher, C.J. Frederickson, Histochemically-reactive zinc in amyloid plaques, angiopathy, and degenerating neurons of Alzheimer's diseased brains, Brain Res. 852 (2000) 274–278.
[8] D.M. Hartley, D.M. Walsh, C.P. Ye, T. Diehl, S. Vasquez, P.M. Vassilev, D.B. Teplow, D.J. Selkoe, Protofibrillar intermediates of amyloid beta-protein induce acute electrophysiological changes and progressive neurotoxicity in cortical neurons, J. Neurosci. 19 (1999) 8876–8884.
[9] H.A. Lashuel, D. Hartley, B.M. Petre, T. Walz, P.T. Lansbury Jr., Neurodegenerative disease: amyloid pores from pathogenic mutations, Nature 418 (2002) 291.
[10] M. Hoshi, M. Sato, S. Matsumoto, A. Noguchi, K. Yasutake, N. Yoshida, K. Sato, Spherical aggregates of beta-amyloid (amylospheroid) show high neurotoxicity and activate tau protein kinase I/glycogen synthase kinase-3beta, Proc. Natl. Acad. Sci. USA 100 (2003) 6370–6375.
[11] W.L. Klein, G.A. Krafft, C.E. Finch, Targeting small Abeta oligomers: the solution to an Alzheimer's disease conundrum? Trends Neurosci. 24 (2001) 219–224.
[12] M.D. Kirkitadze, G. Bitan, D.B. Teplow, Paradigm shifts in Alzheimer's disease and other neurodegenerative disorders: the emerging role of oligomeric assemblies, J. Neurosci. Res. 69 (2002) 567–577.
[13] P.N. Lacor, M.C. Buniel, L. Chang, S.J. Fernandez, Y. Gong, K.L. Viola, M.P. Lambert, P.T. Velasco, E.H. Bigio, C.E. Finch, G.A. Krafft, W.L. Klein, Synaptic targeting by Alzheimer's-related amyloid beta oligomers, J. Neurosci. 24 (2004) 10191–10200.
[14] J.P. Cleary, D.M. Walsh, J.J. Hofmeister, G.M. Shankar, M.A. Kuskowski, D.J. Selkoe, K.H. Ashe, Natural oligomers of the amyloid-beta protein specifically disrupt cognitive function, Nat. Neurosci. 8 (2005) 79–84.
[15] L.F. Lue, Y.M. Kuo, A.E. Roher, L. Brachova, Y. Shen, L. Sue, T. Beach, J.H. Kurth, R.E. Rydel, J. Rogers, Soluble amyloid beta peptide concentration as a predictor of synaptic change in Alzheimer's disease, Am. J. Pathol. 155 (1999) 853–862.
[16] D.M. Walsh, A. Lomakin, G.B. Benedek, M.M. Condron, D.B. Teplow, Amyloid beta-protein fibrillogenesis. Detection of a protofibrillar intermediate, J. Biol. Chem. 272 (1997) 22364–22372.
[17] R.M. Murphy, M.M. Pallitto, Probing the kinetics of beta-amyloid self-association, J. Struct. Biol. 130 (2000) 109–122.
[18] G. Bitan, A. Lomakin, D.B. Teplow, Amyloid beta-protein oligomerization: prenucleation interactions revealed by photo-induced cross-linking of unmodified proteins, J. Biol. Chem. 276 (2001) 35176–35184.
[19] H. Lin, R. Bhatia, R. Lal, Amyloid beta protein forms ion channels: implications for Alzheimer's disease pathophysiology, FASEB J. 15 (2001) 2433–2444.
[20] D. Magde, E. Elson, W. Webb, Thermodynamic fluctuations in a reacting system—measurement by fluorescence correlation spectroscopy, Phys. Rev. Lett. 29 (1972) 705–708.
[21] S. Maiti, U. Haupts, W.W. Webb, Fluorescence correlation spectroscopy: diagnostics for sparse molecules, Proc. Natl. Acad. Sci. USA 94 (1997) 11753–11757.
[22] P. Sengupta, K. Garai, J. Balaji, N. Periasamy, S. Maiti, Measuring size distribution in highly heterogeneous systems with fluorescence correlation spectroscopy, Biophys. J. 84 (2003) 1977–1984.
[23] P. Sengupta, K. Garai, B. Sahoo, Y. Shi, D.J. Callaway, S. Maiti, The amyloid beta peptide (Abeta(1–40)) is thermodynamically soluble at physiological concentrations, Biochemistry 42 (2003) 10506–10513.
[24] P. Sengupta, J. Balaji, S. Maiti, Measuring diffusion in cell membranes by fluorescence correlation spectroscopy, Methods 27 (2002) 374–387.
[25] C.S. Atwood, R.D. Moir, X. Huang, R.C. Scarpa, N.M. Bacarra, D.M. Romano, M.A. Hartshorn, R.E. Tanzi, A.I. Bush, Dramatic aggregation of Alzheimer abeta by Cu(II) is induced by conditions representing physiological acidosis, J. Biol. Chem. 273 (1998) 12817–12826.
[26] C.C. Curtain, F. Ali, I. Volitakis, R.A. Cherny, R.S. Norton, K. Beyreuther, C.J. Barrow, C.L. Masters, A.I. Bush, K.J. Barnham, Alzheimer's disease amyloid-beta binds copper and zinc to generate an allosterically ordered membrane-penetrating structure containing superoxide dismutase-like subunits, J. Biol. Chem. 276 (2001) 20466–20473.
[27] D.S. Yang, J. McLaurin, K. Qin, D. Westaway, P.E. Fraser, Examining the zinc binding site of the amyloid-beta peptide, Eur. J. Biochem. 267 (2000) 6692–6698.
[28] S.T. Liu, G. Howlett, C.J. Barrow, Histidine-13 is a crucial residue in the zinc ion-induced aggregation of the A beta peptide of Alzheimer's disease, Biochemistry 38 (1999) 9373–9378.
[29] J.A. Molina, F.J. Jimenez-Jimenez, M.V. Aguilar, I. Meseguer, C.J. Mateos-Vega, M.J. Gonzalez-Munoz, F. de Bustos, J. Porta, M. Orti-Pareja, M. Zurdo, E. Barrios, M.C. Martinez-Para, Cerebrospinal fluid levels of transition metals in patients with Alzheimer's disease, J. Neural. Transm. 105 (1998) 479–488.
[30] A.I. Bush, The metallobiology of Alzheimer's disease, Trends Neurosci. 26 (2003) 207–214.
[31] D.M. Walsh, D.M. Hartley, Y. Kusumoto, Y. Fezoui, M.M. Condron, A. Lomakin, G.B. Benedek, D.J. Selkoe, D.B. Teplow, Amyloid beta-protein fibrillogenesis. Structure and biological activity of protofibrillar intermediates, J. Biol. Chem. 274 (1999) 25945–25952.